文章编号：1001-9014(2020)05-0533-07

DOI:10. 11972/j. issn. 1001-9014. 2020. 05. 001

# Graphene/GaAs heterostructure based Millimeter/Terahertz wave photodetector

XU Kai-Qi[1], XU Huang[2], ZHANG Jia-Zhen[2], WU Xiang-Dong[2], YANG Lu-Han[2], ZHOU Jie[2], LIN Fang-Ting[1*], WANG Lin[2], CHEN Gang[2*]

(1. Shanghai Normal University, Shanghai 200234, China;
2. State Key Laboratory of Infrared Physics, Shanghai Institute of Technical Physics, Chinese Academy of Sciences, Shanghai 200083, China)

**Abstract**: The low intrinsic absorption and the existence of the inherent defects hamper the monoatomic layer graphene from being a high-performance photoelectric material, which leads to the strategy to form heterostructure by combining graphene with semiconductor materials. In this work, a graphene/GaAs heterostructure based photodetector has been designed and fabricated, in which the two-dimensional electron gas are enhanced to improve the photoresponse ability at the band of sub-millimeter and Terahertz (THz) wave ranging from 20 GHz to 0. 12 THz. Under 25 GHz radiation, the responsivity of photodetector at room temperature (RT) reaches 20. 6 $V\cdot W^{-1}$, with the response time of 9. 8 μs and the noise equivalent power (NEP) of 3. $2\times10^{10}$ $W\cdot Hz^{-1/2}$ under a bias of 400 mV. At 0. 12 THz, the responsivity is determined to be 4. 6 $V\cdot W^{-1}$, with the response time of 10 μs. And a NEP of 1. $4\times10^{-9}$ $W\cdot Hz^{-1/2}$ can be achieved under the bias of 400 mV. These results exhibit great application potential for the graphene/GaAs heterostructure based THz photodetectors.

**Key words**: GaAs-based, HEMT, graphene, Terahertz, heterostructure
**PACS**: :07. 57. Kp, 07. 57. -c, 07. 57. Hm

# 基于石墨烯/砷化镓异质结构的毫米波/太赫兹探测器

徐凯琦[1], 徐 煌[2], 张家振[2], 吴向东[2], 杨露寒[2], 周 洁[2], 林方婷[1*], 王 林[2], 陈 刚[2*]

(1. 上海师范大学,上海 200234;
2. 中国科学院上海技术物理研究所 红外物理国家重点实验室,上海 200083)

**摘要**:单层石墨烯具有较低的固有光吸收效率,且材料中含有较多的缺陷,导致仅依靠石墨烯本身很难制备高性能的光电器件。通过石墨烯与半导体材料复合形成异质结构的方法可以克服这一瓶颈。本工作中利用石墨烯/砷化镓高迁移率异质晶体管结构制备了毫米波光电探测器,有效地提升了二维电子气特性,大幅度提高了器件在室温条件下的毫米波响应和探测能力。实验证明,400 mV 的偏置电压下,该器件在 25 GHz 波段的获得了 20.6 $V\cdot W^{-1}$ 响应率,响应时间为 9.8 μs,噪声等效功率为 $3.2\times10^{-10}$ $W\cdot Hz^{-1/2}$。在太赫兹波 0.12 THz 下响应率仍然达到了 4.6 $V\cdot W^{-1}$,响应时间为 10 μs,噪声等效功率为 $1.4\times10^{-9}$ $W\cdot Hz^{-1/2}$。该工作展示了石墨烯/砷化镓异质结构毫米波太赫兹探测器的巨大应用前景。

**关 键 词**:砷化镓;HEMT;石墨烯;太赫兹;异质结构
**中图分类号**:O473;O434.3 **文献标识码**:A

**Received date**: 2019- 12- 10, **revised date**: 2020- 05- 14 **收稿日期**:2019- 12- 10, **修回日期**:2020- 05- 14
**Foundation items**: Supported by National Natural Science Foundation (61474130) and Shanghai Natural Science Foundation ( 19ZR1465400, 18590780100, 19590711600)
**Biography**: Xu Kaiqi (1995-), He is studying for a master's degree in physics at Shanghai Normal University. The main research field is Graphene/GaAs heterostructure based Millimeter/Terahertz wave photodetection. E-mail: cagekqx@163. com
[*] **Corresponding author**: E-mail: nounou7@163. com, gchen@mail. sitp. ac. cn

## Introduction

Sub-millimeter/THz wave photodetectors, due to its wide application in meteorology, astronomy, medicine, communication and biology[1, 2], have attracted great research interest. Since the photon energy in this regime is comparable to the background thermal noise energy at RT, most reported devices require cryogenic working environment. Conventional semiconductor photodetectors rely on photoexcitation of electron-hole pairs in semiconductors, which is not suitable for detection of sub-millimeter/THz photons. The most used sub-millimeter/THz detectors include Golay cell, thermal electron bolometer, and pyroelectric detectors[3-5]. Due to the thermal sensing mechanism, such detectors are either slow in response since the modulation frequency of Golay batteries and pyroelectric detectors is only a few hundred hertz, or must be cooled with liquid Helium. In contrast, Schottky barrier diodes (SBD), which exhibit high-speed response at RT, require the use of complex techniques in device fabrication and material production. As a result, their chip integration is currently being hampered. Therefore, there is an urgent need for a new detection scheme that can provide both fast response, RT operation, high sensitivity, and ease of manufacture. In the past few years, great efforts have be devoted to the development of field effect transistor based millimeter and THz photodetectors[6].

Sub-millimeter and THz field effect transistors usually have submicron-scaled channel[2,4-5,7]. In the transistor, photon absorption can be enhanced by a well-designed source-gate antenna, which leads to longitudinal electric field along channel to drive electrons resonant. Thus a DC signal can be measured between the source and drain($V_{ds}$). A photo-conductor, such as GaAs, possessing high resistivity and ultra-short carrier lifetime in connection with the antenna, confines incident light and generate electric field at the interface between it and antenna. Meanwhile, photo-excited carriers form photocurrent in proportion to the intensity of incident light field[6, 8, 9], driven by the force of the generated electric field.

Graphene and other two-dimensional materials have been proven competent to detect long-wavelength photons in recent years[4, 10-13]. Graphene detectors, including field effect transistors[4], thermal electron side bolometers[13], and photo-thermal electric devices[11], have seen a great development in the last couple of years. Graphene field effect transistor-based detectors perform well at RT and in the 300GHz band[4]. The reported two-layer graphene hot electron side bolometer has almost comparable sensitivity as silicon devices at low temperatures but faster response[13]. At RT, graphene sub-millimeter/terahertz detector showing detectivity greater than 10 V/W and half-height width pulse of 110 ps[11]. In addition, a long-wave detector based on carrier thermal transfer at temperature < 30K has also been reported[14]. It is capable to respond to 55μm-wavelength radiation. To further enhance the performance of the graphene based photodetectors, the hybrid structured devices based on the van der Waals (vdW) heterostructure has been well developed[15]. For example, GaAs/Graphene hetero-structure optoelectronic devices have attracted a lot of attention, due to the outstanding electrical and optical properties in wavelength-independent absorption, low dissipation rate, extraordinarily high carrier mobility, and micro-scale ballistic transport[15-21]. On the other hand, there has yet been any report on the GaAs/Graphene based sub-millimeter/THz photodetector, thus in this work, we designed and fabricated a graphene/GaAs heterostructure based photodetector, and the results of the photoresponse in the range of sub-millimeter and terahertz range are reported to verify the availability to achieve higher THz response with the vdW heterostructure.

## 1 Experimental

The high mobility GaAs sample was prepared with molecular beam epitaxial (MBE) method. Semi-insulating n-type GaAs wafer is used as the substrate. The growth is performed with a Riber-21 MBE system. After a high temperature adsorption of the substrate, a 50 nm GaAs layer, with the Si doping concentration of $2\times10^{17}\,cm^{-3}$, is deposited at 600℃ with growth rate of 0.21 nm/s. Then the sample is taken out of the MBE chamber, and is cleaned using an ultrasonic treatment with acetone solution, isopropanol solution and deionized water. After drying with nitrogen, the sample is placed in oven, and is baked at 120 °C for another 2 hours.

Before transferring the graphene layer, a 10-nm-thick GaAs layer is etched away from the sample with a standard GaAs etching solution ($H_3PO_4$: $H_2O_2$: $H_2O$ = 40: 20: 400 ml). After that, single-layer graphene is transferred upon the substrate with a well-developed method[21]. Then we transferred a monolayer graphene sheet onto this substrate, which initially is grown on copper foil. The specific transfer process of graphene is as follows: Firstly, a layer of PMMA is spin coated onto the graphene film. Then it is put into a solution of ferric chloride ($FeCl_3$) to etch the copper foil. After the copper foil is etched completely, it will be taken out and put into a dilute hydrochloric acid solution. The PMMA covered graphene is subsequently fished out by GaAs substrate. Finally, dip the hybrid graphene/GaAs sample is dipped into acetone solution to remove PMMA, and then it is further rinsed with isopropyl alcohol, and dried in the air.

Then the electrode source and drain are deposited (Cr/Au 5/60 nm) with ultraviolet lithography and electron beam evaporation. Graphene is etched with $O_2$ plasma treatment to obtain designed channel size. After that, a 30nm-thick gate dielectric $Al_2O_3$ layer is deposited in ALD process. At last, electrode gate is deposited with ultraviolet lithography and electron beam evaporation process.

The IV characteristics of the devices were measured by B2912A Semiconductor Analyzer using variable voltage mode. For photoresponse measurements, the sub-millimeter/THz waves at different frequencies were generated from multiplier of electronic source and the photovoltage data were collected by B2912A and magnified by

a lock-in amplifier and preamplifier. The 0.12 THz source based on frequency multipliers was employed in the photoresponse experiments. And the power density of the millimeter wave is 2.5 mW·cm$^{-2}$, the power density of the sub-millimeter/THz radiation was 1.05 mW·cm$^{-2}$ calibrated by a Golay cell. The detailed measurement setup can found in our previous work[22, 23].

## 2 Results and discussion

Fig. 1(a), (b) are the cross-sectional structural schematic and the corresponding optical top view of the fabricated device, respectively. Here, the graphene channel length is L = 6 μm. To enhance the absorption at wavelength of millimeter scale, a bow-tie antenna with subwavelength gap is contacted to the detecting material to form the channel. The length and the width of the bow-tie antenna defined region are 200 μm and 140 μm, respectively, as shown in Fig. 1(b). In Fig. 1(c) Raman spectrum of the monolayer graphene shows two strong peaks: 2D peak (2680 cm$^{-1}$) and G peak (1580 cm$^{-1}$), which indicates the high quality of the monolayer graphene, since 2D/G intensity ratio is about 2.9. The D peak at 1350 cm$^{-1}$) is caused by the disorder induction and defect of graphene. The peak value is small, indicating that the quality of transferred graphene is high[24-26]. As shown in Fig. 1(d), the transfer characteristic curve of the detector shows a bipolar behavior[27]. The neutral charge point (CNP) is located at $V_g$ (gate voltage) = 2.2 V, indicating that graphene is p-type.

Fig. 2(a) (b) are the time response of the photocurrent under radiation of 25 GHz at modulation frequencies of 1 kHz and 10 kHz with zero bias. Fig. 2(c) is the photocurrent response as a function of incident power at different bias voltages. It can be seen that the photocurrent increases almost linearly with the incident light power, which is due to fact that the higher the incident light power, the more pairs of electron-hole and excitons are generated. Fig. 2 (d) shows the time response of the photocurrent at different bias voltage. The time response is still smooth at the modulation frequency reached 1kHz and 10 kHz. It indicated that the response performance of the device is at μs level, which will be discussed later.

Fig. 3(a) is the extension of the rising edge and falling edge (inset) of the photocurrent in a single time-period. And the rising time and falling time are 9.8 μs and 2 μs, respectively, which is usually defined as the time measured from 10% up to 90% on rising edge of signal as well as the recovery time from 90% down to 10% of the falling edge. In the meantime, the response speed is also much faster than the typical RT thermal-based photodetectors such as the pyroelectric and bolometric ones,

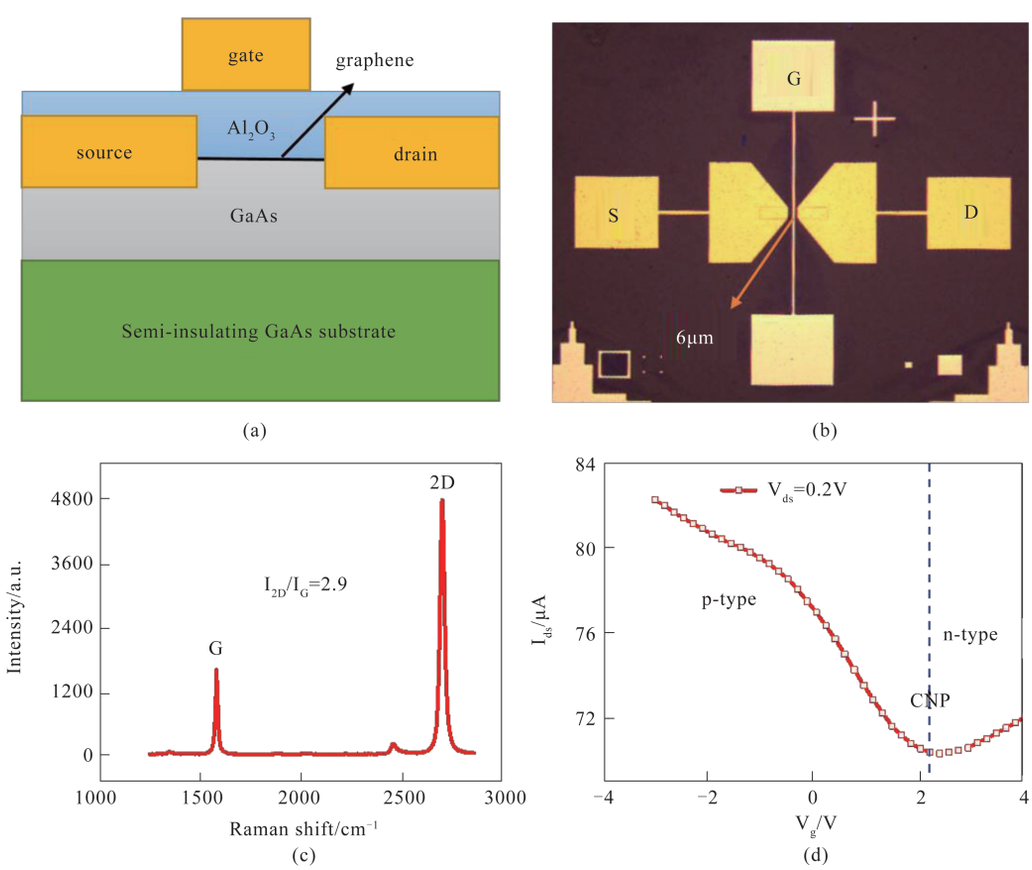


Fig. 1　(a)(b) the cross-sectional structural schematic and the corresponding optical top view of the fabricated device (c) Raman spectrum of the monolayer graphene (d) transfer characteristic curve measured with $V_{ds}$ = 0.2V

图 1　(a)(b)该器件的横截面结构示意图和光学俯视图 (c)单层石墨烯的拉曼光谱图(d)当 Vds = 0.2V 时转移特性曲线

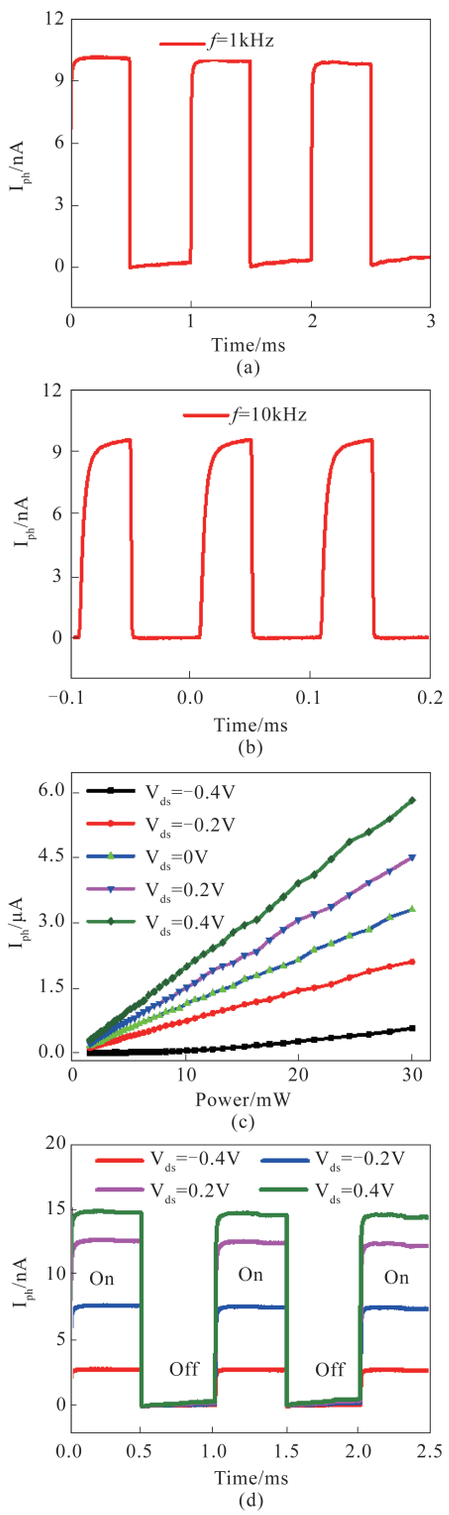


Fig. 2 (a)(b) Time response of the photocurrent under radiation of 25 GHz at modulation frequencies of 1kHz and 10kHz with zero bias (c) Photocurrent response as a function of incident power at different bias voltages (d) Time response of the photocurrent at different bias voltage

图2 (a)(b) 25 GHz辐照下,零偏压下调制频率为1kHz,10kHz时,光电流随时间的变化(c)不同偏压下光电流随微波功率的变化(d)不同偏压下光电流随时间的变化

which response to the radiation on the order of ms. Fig. 3 (b) is the photocurrent as a function of the gate voltage with $V_{ds}$ of 0.2 V, which will be discussed with Fig. 5(b) together later. It can be seen from Fig. 3(c) that when the forward bias increases, the photocurrent increases almost linearly. And when reverse bias increases, the photo-current decreases linearly as well. Responsivity ($R_v$) and noise equivalent power (NEP) are two important parameters for photodetectors. Usually, a responsivity of $R_i$ can be obtained from the equation $R_i = (S_b \cdot I_{ph}) / (P_{in} \cdot S_\lambda)$ at zero bias. Here $P_{in}$ is the total power of the source, $S_b$ is the radiation beam spot area, and $S_\lambda$ is the active area. Nevertheless, given the fact that the wavelength λ corresponding to the 25 GHz is about 12 mm, which is much larger than the device itself. Thus an alternative method to calculate the responsivity has to be used for the sub-wavelength case[4], in which, the responsivity can be expressed by $R_i = (S_b \cdot I_{ph}) / (P_{in} \cdot S_\lambda')$, where the $S_\lambda' = \lambda^2/4$. By this method, the $R_i$ can be determined to be about 4.1 mA/W. Since the $R_v = R_i \cdot R$, $R$ = 2.6 kΩ is the resistance of the device, the $R_v$ = 10.7 V/W can be obtained. When the photocurrent reaches ($I_{ph}$) 6.16 μA, the $R_v$ of the device can be determined to be 20.6 V/W under $V_{ds}$ = 0.4 V. According to the noise equivalent power formula NEP = $(4TRK_B)^{1/2} / R_v$, where $K_B$ is the Boltzmann constant, $T$ is the temperature, $R$ is the device resistance[28-31], the noise equivalent power (NEP) of the device at RT can reach below $3.2\times10^{-10}$ W/Hz$^{1/2}$.

Fig. 4(a) (b) (c) show the time response of the device under radiation of 0.12 THz at different modulation frequencies of 1kHz, 5kHz and 10kHz under zero bias, respectively. Fig. 4(d) is the time response of the photodetector at different bias voltage with different modulation frequencies of 1kHz. As can be seen from the Fig. 4, the photodetector is extremely sensitive to terahertz radiation with fast response speed, and maintains a complete pulse shape at modulation frequency of 10 kHz, which indicates stable temporal response performance.

Fig. 5(a) is the extension of the rising edge and falling edge (inset) of the photocurrent in a single time-period, in which the response time are 11 μs and 10 μs under radiation of 0.12THz. Fig. 5(b) shows photocurrent variation as a function of gate voltage with $V_{ds}$ of 0.4 V, in which the highest photocurrent reaches 113nA. Based on the obtained photocurrent, the photoresponsivity at different $V_{ds}$ can be determined as shown in Fig. 5(c). With 0.12 THz radiation, the λ is 2.5mm, and thus the responsivity at RT can reach 4.6 V/W at $V_{ds}$ of 0.4 V. Similarly noise equivalent power can also be deduced and exhibited in Fig. 5(d) as a function of the gate voltage $V_g$, which shows the lowest NEP is less than $1.4\times10^{-9}$ W Hz$^{-1/2}$.

As shown in Fig. 3(b) and 5(b), the photocurrent of is mainly generated due to the intraband excitation of graphene. The contact potential does not contribute much to the photocurrent. It is necessary to consider the influence of high concentration carriers in GaAs on the photoresponse of graphene.

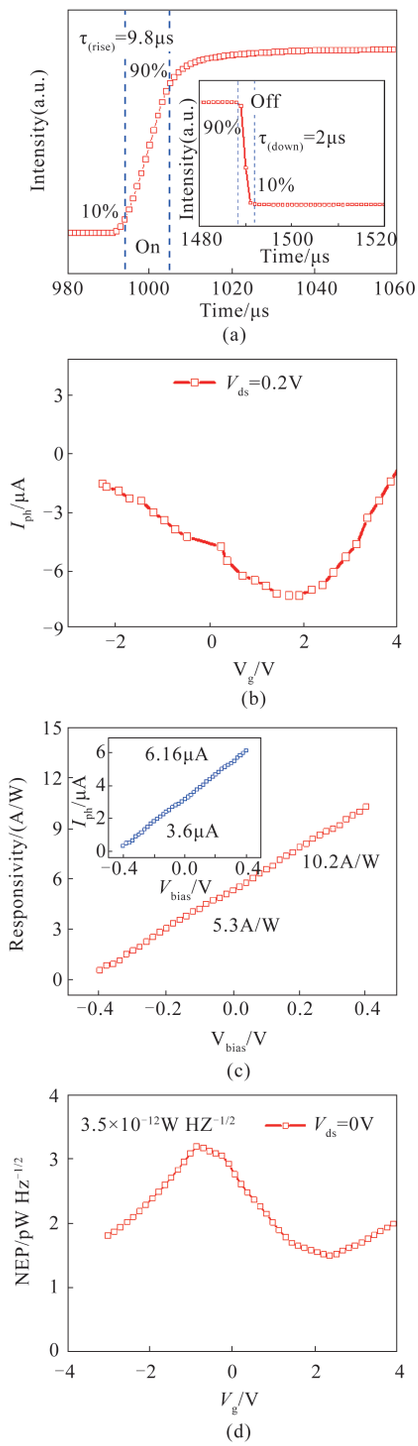


Fig. 3　(a) The extension of the rising edge and falling edge (inset) of the photocurrent in a single time-period (b) Photocurrent as a function of the gate voltage with $V_{ds}$ of 0.2 V (c) Photoresponsivity at different bias voltage (d) Noise equivalent power variation with gate voltage

图3　(a) 单个周期内光电流的上升沿和下降沿 (b)$V_{ds}$=0.2 V时,光电流随着栅压的变化(c)响应率和光电流随偏压的变化(d) 噪声等效功率随栅压变化。

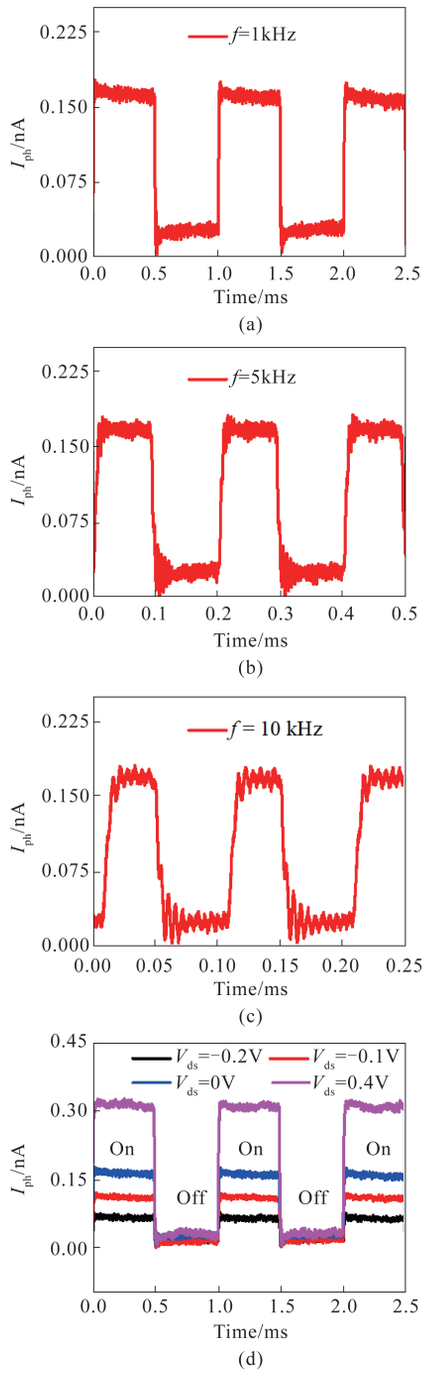


Fig. 4　(a) (b) (c) The time response of the device under radiation of 0.12 THz at different modulation frequencies of 1kHz, 5kHz and 10kHz under zero bias (d) The time response of the photodetector at different bias voltage at different modulation frequencies of 1kHz

图4　(a)(b)(c) 在0.12THz下,零偏压下调制频率为1kHz,5kHz,10kHz时,探测器的时间响应 (d)调制频率为1kHz时,加偏压为-0.2V,-0.1V,0V,0.4V,探测器的时间响应

To explore the mechanism behind the phenomena observed in the heterostructure-based photodetector, a schematic is proposed in Fig. 6, based on the measured responsivity as shown in Fig . 1 and Fig. 3. Due to the nature of the hybrid channel of our device, the measured transfer characteristics is not only determined by the graphene[22-24,32-34], but also influenced by the graphene-GaAs heterostructure[24,28].

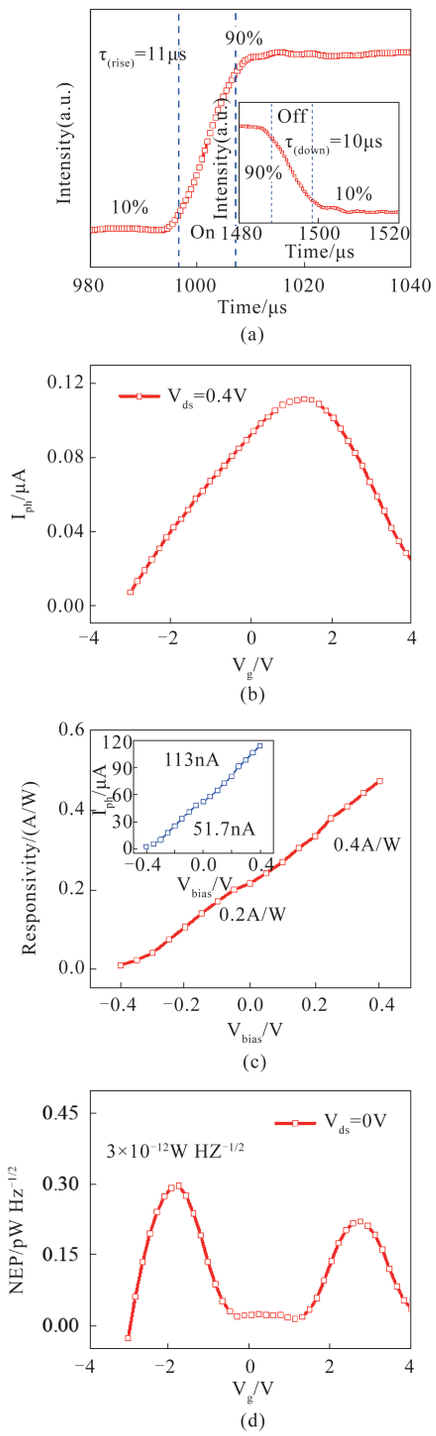


Fig. 5 (a) The extension of the rising edge and falling edge (inset) of the photocurrent in a single time-period (b) Photocurrent variation as a function of gate voltage with $V_{ds}$ of 0.4 V (c) Photoresponsivity obtained at different bias voltage $V_{ds}$ (d) Noise equivalent power variation with the gate voltage $V_g$

图5 (a) 在单个周期内光电流的上升沿和下降沿的外延(b) Vds=0.4V,光电流随着栅压的变化(c)光电流和响应率随偏压变化 (d) 噪声等效功率随栅压变化

When the graphene is in contacting with GaAs, a contact potential well is formed, which leads to the accumulation of a number of carriers at the well. And the

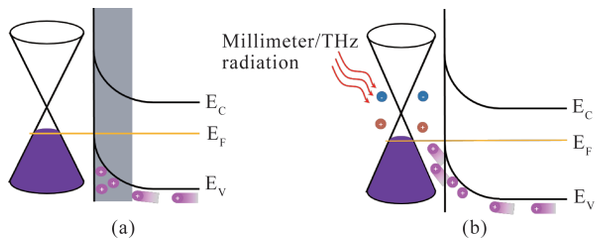


Fig. 6 Schematic energy band diagrams of graphene /GaAs hetero-structure (a) without millimeter/THz radiation; and (b) under millimeter/THz radiation

图6 石墨烯/砷化镓异质结构探测器随毫米波/太赫兹辐照的变化的能带示意图 (a) 无辐照 (b) 有辐照。

change in the size of the well will affect the carrier behavior between the source and the drain. Without millimeter/THz radiation, when $V_{ds} = 0.2$ V, and $V_g < 0$, as shown in Fig. 1(c), the graphene Fermi level rises, leading to the rise of both of the barrier height between the graphene and the GaAs. Thus the carrier concentration at the potential well increases subsequently, resulting in the photocurrent $I_{ds}$ increases as well, as indicated in the Fig. 6(a). On the other hand, when $0 < V_g < 2.2$ V, the graphene Fermi level decreases, which lowers the barrier as well as the carrier concentration, and the source and drain current decreases subsequently. Further increase the $V_g$ above the neutral charge point of 2.2 eV, the inversion onsets, in which case, the graphene becomes n type, and the carrier concentration increases again.

On the other hand, under the radiation, the photocurrent of the photodetector is mainly generated by the in-band excitation of graphene, as indicated in Fig. 6(b). When $V_g$=0, the carriers accumulated in the contact well have a certain gain effect on the photocurrent due to the positive effect of the high concentration carriers in GaAs. When $V_g$<0, the potential well increases, and carriers at the potential well are difficult to migrate, which reduces the potentiation on the graphene photocurrent, and the photocurrent decreases. On the contrary, when $V_g$>0, the potential well is reduced, and the photocurrent potentiation on graphene is remarkable. When $V_g > V_{(CNP)}$, the photocurrent decreases, and changes to the contrary. Thus the results exhibited in Fig. 3 can be well understood.

## 3 Conclusion

In this work, a graphene/GaAs heterostructure based photodetector has been designed and fabricated, in which the two-dimensional electron gas characteristics are enhanced to improve the photoresponsivity at the band of millimeter and THz wave ranging from 20 GHz to 0.12 THz. Under 25 GHz radiation, the responsivity of photodetector at room temperature (RT) reaches 20.6 $V \cdot W^{-1}$, with the response time of 9.8 μs and the noise equivalent power (NEP) of $3.2 \times 10^{10}$ $W \cdot Hz^{-1/2}$ under a bias of 400 mV. At 0.12 THz, the responsivity is determined to be 4.6 $V \cdot W^{-1}$, with the response time of 10 μs. And a NEP of $1.4 \times 10^{-9}$ $W \cdot Hz^{-1/2}$ can be achieved under the bias of 400 mV. To further improve the perfor-

mance the GaAs/Graphene hetero-structured photodetector, various approaches will be adopted, such like optimization of the antenna, and the reducing the length of the channel, both to enhance the coupling of the electromagnetic field in the channel. These results exhibit great application potential for the graphene/GaAs heterostructure based Terahertz photodetectors.

## Acknowledgment

This work is sponsored by the National Natural Science Foundation of China (61474130), the Natural Science Foundation of Shanghai via 19ZR1465400, and the Science and Technology Commission of Shanghai Municipality (18590780100, 19590711600).

## References

[1] Monch, W. On the physics of metal-semiconductor interfaces[J]. *Reports on Progress in Physics* 1990, **53** (3): 221-278.
[2] Liu H, Song C, Springthorpe A, *et al*. Terahertz quantum-well photodetector[J]. *Applied Physics Letters* 2004, **84** (20): 4068-4070.
[3] Kopylov S, Tzalenchuk A, Kubatkin S, *et al*. Charge transfer between epitaxial graphene and silicon carbide[J]. *Applied Physics Letters* 2010, **97**(11).
[4] Vicarelli L, Vitiello M S, Coquillat D, *et al*. Graphene field-effect transistors as room-temperature terahertz detectors[J]. *Nature Materials* 2012, **11** (10): 865-871.
[5] Knap W, Teppe F, Meziani Y, *et al*. Plasma wave detection of sub-terahertz and terahertz radiation by silicon field-effect transistors[J]. *Applied Physics Letters* 2004, **85** (4): 675-677.
[6] Peng K, Parkinson P, Fu L, *et al*. Single Nanowire Photoconductive Terahertz Detectors[J]. *Nano Letters* 2015, **15** (1): 206-210.
[7] Dyakonov, Michael , M. Shur . Shallow water analogy for a ballistic field effect transistor: New mechanism of plasma wave generation by dc current[J]. *Physical Review Letters* 1993, **71**(15): 2465-2468.
[8] Berry C W, Wang N, Hashemi M R, *et al*. Significant performance enhancement in photoconductive terahertz optoelectronics by incorporating plasmonic contact electrodes [J]. *Nature Communications* 2013, 4.
[9] Castro-Camus E, Lloyd-Hughes J, Johnston M B, *et al*. Polarization-sensitive terahertz detection by multicontact photoconductive receivers[J]. *Applied Physics Letters* 2005, **86**(25).
[10] Koppens F H L, Mueller T, Avouris P, *et al*. Photodetectors based on graphene, other two-dimensional materials and hybrid systems [J]. *Nature Nanotechnology* 2014, **9**(10): 780-793.
[11] Cai X, Sushkov A B, Suess R J, *et al*. Sensitive room-temperature terahertz detection via the photothermoelectric effect in graphene[J]. *Nature Nanotechnology* 2014, **9**(10): 814-819.
[12] Viti L, Hu J, Coquillat, Dominique..*et al*. Black Phosphorus Terahertz Photodetectors[J]. *Advanced Materials* 2015, **27**(37): 5567-5572.
[13] Yan J, Kim M H, Elle J A, *et al*. Dual-gated bilayer graphene hot-electron bolometer [J]. *Nature Nanotechnology* 2012, **7** (7): 472-478.
[14] Lao Y F, Perera A G U, Li L H, *et al*. Tunable hot-carrier photodetection beyond the bandgap spectral limit [J]. *Nature Photonics* 2014, **8**(5): 412-418.
[15] Hong Y J, Yang J W, Lee W H, *et al*. Van der Waals epitaxial double heterostructure: InAs/single-layer graphene/InAs [J]. *Advanced Materials* 2013, **25**(47): 6914-6914.
[16] Chen S, Han Z, Elahi M M, *et al*. Electron optics with p-n junctions in ballistic graphene[J]. *Science Letter*, 2016, **353**(6307): 1522-1525.
[17] Geim A K J S. Graphene: status and prospects[J]. *science*, 2009, **324**(5934): 1530-1534.
[18] Li X, Chen W, Wang P, *et al*. 18.5% Efficient graphene/GaAs van der Waals heterostructure solar cell[J]. *Nano Energy*, **2015**, 16: 310-319.
[19] Nair R R, Blake P, Grigorenko, *et al*. Fine structure constant defines visual transparency of graphene [J]. *Science*, 2008, **320** (5881): 1308-1308.
[20] Rezgui K, Othmen R, Cavanna A, *et al*. The improvement of InAs/GaAs quantum dot properties capped by Graphene[J]. *Journal of Raman Spectroscopy*, 2013, **44**(11): 1529-1533.
[21] Wu J, Yang Z, Qiu C, *et al*. Enhanced performance of a graphene/GaAs self-driven near-infrared photodetector with upconversion nanoparticles[J]. *Nanoscale*, 2018, **10**(17):8023-8030.
[22] Jiang M, Xiao H Y, Peng S M, *et al*. A comparative study of low energy radiation response of AlAs, GaAs and GaAs/AlAs superlattice and the damage effects on their electronic structures[J]. *Scientific reports*, 2018, **8**(1): 2012.
[23] Liu Q L, Zhao Z Y, Yi J H. Interfacial interaction and effects of GaAs/Graphene hetero-structures studied by First-principle calculations[J]. *Journal of Alloys and Compounds*, 2019, **795**:351-360.
[24] Hu Zhi Ting, Gan Tao, Du Lei, *et al*. A novel photodetector based on Graphene/InAs quantum dots/GaAs hetero-junction [J]. *Journal of Infrared and Millimeter Waves*, 2019, **38**(3).
[25] Ferrari A C, Meyer J C, V. Scardaci, *et al*. Raman spectrum of graphene and graphene layers[J]. *Phys Rev Lett* 2006, **97**(18): 187401.
[26] Malard L M, Pimenta M A, Dresselhaus G, *et al*. Raman spectroscopy in graphene[J]. *Physics Reports* 2009, **473**(5-6): 51-87.
[27] Tuinstra F, Koenig J L. Raman Spectrum of Graphite[J]. *The Journal of Chemical Physics* 1970, **53**(3): 1126-1130.
[28] Yang X, Sun J, Qin, *et al*. Room-temperature terahertz detection based on CVD graphene transistor[J]. *Chinese Physics B*, 2015, **24** (4):47206-047206.
[29] Richards P L. Bolometers for infrared and millimeter waves[J]. J. *Appl. Phys*. 1994, **76**(1): 1-24.
[30] Tauk R, Teppe F, Boubanga S, *et al*. Plasma wave detection of terahertz radiation by silicon field effects transistors: Responsivity and noise equivalent power[J]. *Applied Physics Letters*, 2006, **89**(25).
[31] Tang W, Politano A, Guo C, *et al*. Ultrasensitive Room-Temperature Terahertz Direct Detection Based on a Bismuth Selenide Topological Insulator[J]. *Advanced Functional Materials*, 2018, **28**(31): 1801786.
[32] Liu C, Du L, Tang W, *et al*. Towards sensitive terahertz detection via thermoelectric manipulation using graphene transistors. *Npg Asia Materials*, 2018, 10: 318-327.
[33] Wu J, Yang Z, Qiu C, *et al*. Junction investigation of graphene/silicon Schottky diodes[J]. *Nanoscale research letters*, 2012, **7**(1), 302-302.
[34] Mark H. Rümmeli, Rocha C G, Ortmann F,*et al*. Graphene: Piecing it together[J]. *Advanced Materials*, 2011, **23**(39), 4471-4490.